Chinese Chemical Letters 34 (2023) 107866

Contents lists available at ScienceDirect

Chinese Chemical Letters

journal homepage: www.elsevier.com/locate/cclet

Construction of AIEgen functionalized nanomicelles and their stability study through 'seesaw-like' fluorescence changes

Xiaotong Wang[a,1], Shizhu Chen[a,1], Yaru Jia[b], Kaihan Zhang[c], Lili Ma[a], Luwei Li[a,*], Xingjie Liang[b,*], Jinchao Zhang[a,*]

[a] College of Chemistry and Environmental Science, Chemical Biology Key Laboratory of Hebei Province, Key Laboratory of Medicinal Chemistry and Molecular Diagnosis of the Ministry of Education, Hebei University, Baoding 071002, China
[b] CAS Key Laboratory for Biomedical Effects of Nanomaterials and Nanosafety, CAS Center for Excellence in Nanoscience, National Center for Nanoscience and Technology of China, Beijing 100190, China
[c] Department of Chemistry, The University of Manchester, Manchester M13 9PL, United Kingdom

ARTICLE INFO

Article history:
Received 25 May 2022
Revised 21 September 2022
Accepted 28 September 2022
Available online 1 October 2022

Keywords:
Polymer nanomicelles
Aggregation-induced emission
Fluorescence ratio
Stability
Drug delivery system

ABSTRACT

As nanocarriers, nanomicelles play vital roles in the toolbox of drug delivery. The stability of nanomicelles affects the nanomedicines' bioactivity. Therefore, it is important to understand the stability of nanomicelles for further improvements. Here, we report a strategy to construct new nanomicelles (NM) by introducing aggregation-induced emission (AIE) functional group tetraphenylethylene (TPE) in the component polymer vitamin E (D-α-tocopheryl polyethylene glycol 1000 succinate) (TPGS). The stability of doxorubicin (DOX) loaded nanomicelles DOX@NM in different conditions was studied by fluorescence analysis. The fluorescence changes of DOX@NM are 'seesaw-like' when they transform between assembled and disassembled forms. In the assembled form, TPE gives emission from AIE effect, while in the disassembled form, the fluorescence of DOX is observed due to the disappearance of ACQ effect.

Nanomedicines, with different kinds of nanocarriers such as micelles [1,2], liposomes [3,4], polymers [5,6], dendrimers [7,8], or even inorganic nanoparticles [9,10], gain increasing attentions for the nanoparticles' inherited merits such as enhanced permeability and retention (EPR) effect in drug delivery [11,12]. Among these nanocarriers, micelles is a kind of 'hot' tool, for their fast accumulation into tumors due to their smaller size, high efficacy, and liable functionalization with peptides, aptamers *etc.*, for targeting and improving the pharmacological performance of payloads [13–15]. Several micellar drugs such as Genexol® PM, Nanoxel® M and Cequa®, have achieved clinical transformation [16,17]. *In vivo*, many factors might affect the transporting and target releasing of nanomedicines [18], such as pH values [14], different biomolecules or proteins [19]. Hence, stability issues are still challenges that hinder micellar nanomedicines in clinical [20,21]. Therefore, it is indispensable to have a better understanding of the stability of micellar nanomedicine.

To evaluate micellar drugs' stability, some strategies are commonly used. The first strategy is to introduce chromophore dyes on nanomicelles. The chromophore dyes are used to track the location of nanomicelles in cells [22]. However, due to the aggregation-caused quenching (ACQ) effect, when their concentration increased, their fluorescent intensity decreased. Moreover, the dynamic changes of micelles could not be monitored by fluorescence in real-time. These limitations impede their applications [23]. The second strategy is based on Förster resonance energy transfer (FRET) [24]. It can be used to monitor the dynamic change of micelles based on the donor and acceptor distances [25]. ACQ effect also limits its applications. The third strategy is to use the radiolabeling method by introducing molecules with easily detectable radionuclides. Although the radiolabeling method avoids the ACQ effect [26], the changes of the signal are only associated with radiolabeled molecules. It is difficult to reflect the states of micelles. These existing strategies are not satisfactory when evaluating the stability of micelles.

Aggregation-induced emission (AIE) is an important photophysical phenomenon [27,28]. They have shown potential applications in biological probes [29], chemical sensing [30], optoelectronic systems [31], stimuli responses, *etc.* [32]. Taking the advantages of the AIE effect, diverse sensing systems have been studied, such as in

* Corresponding authors.
E-mail addresses: liluwei@hbu.edu.cn (L. Li), liangxj@nanoctr.cn (X. Liang), jczhang6970@163.com (J. Zhang).
[1] These authors contributed equally to this work.

https://doi.org/10.1016/j.cclet.2022.107866
1001-8417/

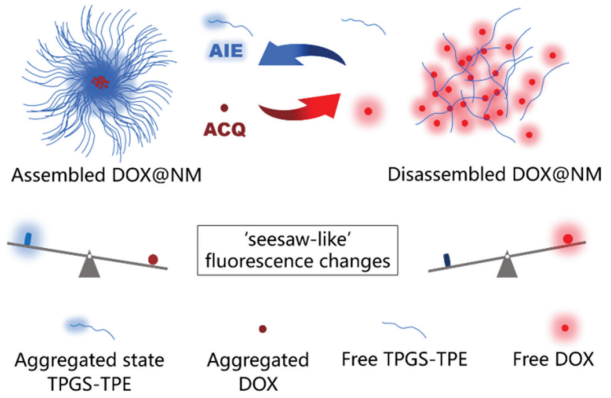

Scheme 1. 'Seesaw-like' fluorescence changes of the DOX@NM.

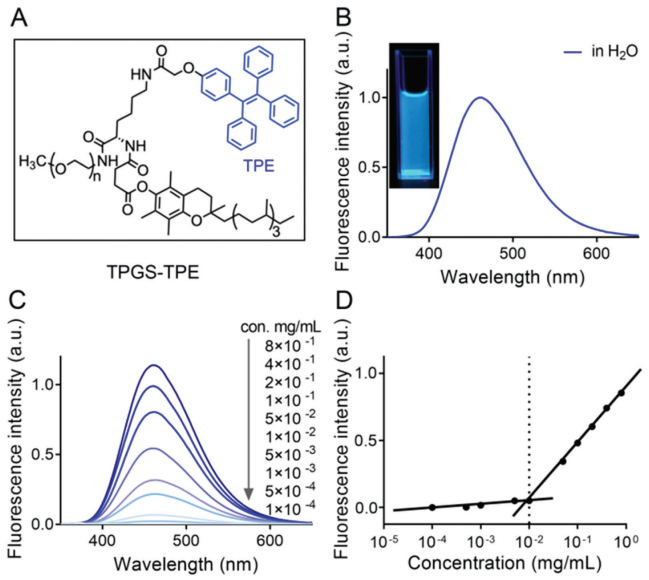

Fig. 1. (A) The structure of TPGS-TPE; (B) Fluorescence spectra of TPGS-TPE in H_2O; (C) Fluorescence spectra of TPGS-TPE at different concentrations (mg/mL) in H_2O; (D) Plot of critical micelle concentration.

the fields of visualization of drug delivery [33], release [34], and distribution *in vivo* [35]. However, to the best of our literature studying, there have been no reports using AIE-based sensors to evaluate micelles' stability.

Here, we report rational designed structural self-indicating nanomicelles (NM) based on AIE functionalized polymers (TPGS-TPE) to study the stability of nanomicelles. The fluorescence changes of doxorubicin (DOX) loaded nanomicelles DOX@NM are 'seesaw-like' when they transform between assembled and disassembled forms as illustrated in Scheme 1. The structure of TPGS-TPE is shown in Fig. 1, and the synthetic procedure can be found in Scheme S1 (Supporting information). With a lipophilic alkyl tail and hydrophilic polar head, TPGS has shown wide application potential in nanocarrier drug delivery systems [36]. TPE (Ex = 330 nm, Em = 460 nm, in the aggregate state) is introduced as AIEgens. In TPE, four phenyl rings are linked to a central ethenyl group. When the NM was in assembled state, the hydrophobic TPE aggregated in the cores of NM. The intramolecular rotations of TPE are restricted due to the physical constraint. It blocks the radiationless relaxation channel and opens the radiative decay pathway [37]. As a result, TPE molecules emit strong blue fluorescence when aggregated.

TPGS-TPE was synthesized and characterized by ^{1}H NMR, MALDI-TOF, IR, and GPC, which confirm the successful synthesis (Figs. S1-S3 and Table S1 in Supporting information). When the fluorescence of TPGS-TPE was explored, it was found that in DMSO, TPGS-TPE did not exhibit fluorescence. However, when we use H_2O as the solvent, TPGS-TPE are aggregated and assembled into NM. Under 330 nm UV light, Intense blue fluorescence with emission wavelength at 460 nm was observed (Fig. 1B). After 1 h of irradiation, the fluorescence intensity remained above 99%, which proved NM's good UV stability in H_2O (Fig. S4 in Supporting information). Besides, the fluorescence intensities in different concentrations were determined. With the decrease of TPGS-TPE concentration from 8×10^{-1} mg/mL to 1×10^{-4} mg/mL, the fluorescence intensity gradually decreased (Fig. 1C). The critical micelle concentration (CMC) of TPGS-TPE is 1×10^{-2} mg/mL (Fig. 1D), which is slightly higher than pure TPGS, 6.63×10^{-3} mg/mL (0.01 mmol/L) [38].

Next, we studied the drug loading property of NM. We chose DOX (Ex = 480 nm, Em = 590 nm) as the model drug (Fig. S5 in Supporting information). DOX was loaded into the NM by the thin film hydration method. Uniform transparent red drug-bearing micelle solutions were formed. In TEM, spherical shape DOX@NM could be observed (Fig. S6 in Supporting information). We optimize the preparation with TPGS-TPE:DOX = 10:1. The hydrated particle size is about 138 ± 3 nm (Fig. S7A in Supporting information) with a surface charge of −14.5 mV (Fig. S7B in Supporting information). The DOX loading capacity and encapsulation rates were 98% and 9%, respectively in Table S2 (Supporting information). It is stable in an aqueous solution over 30 days (Fig. S8 in Supporting information). The pH effects of DOX@NM were explored. It was found that at pH 7.4, a neutral condition of the physiological environment, the DOX release rate was around 60% in 48 h. When the pH decreased to 5.5, the release of the drug was accelerated to nearly 90% in 48 h (Fig. S9 in Supporting information). This indicates the drug release process is pH sensitive. It might benefit the anticancer ability of DOX@NM. The following pharmacodynamic evaluation was taken using DOX@NM against MCF-7S (DOX sensitive cells) and MCF-7R (DOX resistant cells) cell lines (Figs. S10-S13 and Table S3 in Supporting information). DOX@NM exhibited superior cytotoxicity (MCF-7R, IC_{50} = 6.24 μg/mL) compared to free DOX (MCF-7R, IC_{50} = 25.13 μg/mL). Besides, the 'seesaw-like' fluorescence intensity changes between the DOX and TPE are observed in this process.

In our opinion, solvents are important factors that affect the DOX release from the DOX@NM. Different solvents' effects on DOX@NM were studied. Starting with pure H_2O, with an increased proportion of DMSO in H_2O, the hydrophobic driving force in DOX@NM assembly dissipates, leading to the disintegration of DOX@NM. And the corresponding AIE fluorescence at 460 nm gradually disappears. Meanwhile, DOX was released from DOX@NM, and the fluorescence of DOX molecule at 590 nm gradually recovered, presenting a 'seesaw-like' trend (Figs. 2A and B). When the DMSO portion reached 90% (Fig. 2C), the DOX@NM was completely disassembled and turned to a completely non-aggregated state. The AIE phenomenon of TPE molecule disappeared completely; meanwhile, the DOX molecule existed in a free from. The fluorescence of DOX recovered completely. This fluorescence 'seesaw-like' behavior is also worked in different solvent systems, such as 1,4-dioxane, ethanol, and DMF (Figs. S14 and S15 in Supporting information).

Based on these 'seesaw-like' fluorescence changes during the DOX@NM disassembling process, we plotted a DOX@NM status coordinate chart using organic solvent/H_2O ratio as the X-axis, and the fluorescence intensity ratio of DOX/TPE (590 nm/460 nm) as the Y-axis, which as an indication of the state of DOX@NM. In the coordinate plot, at different ratios to H_2O, DMSO, 4-dioxane, ethanol, and DMF solvents system plots are all presented in S-shape (Fig. 2D). The process could be roughly divided into three stages: (i) assembled, (ii) disassembling and (iii) complete disas-

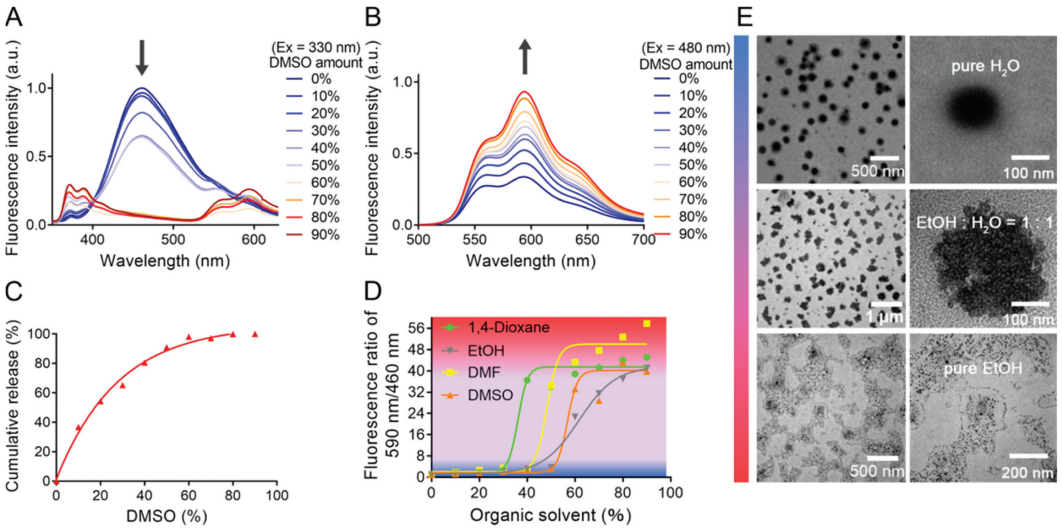

Fig. 2. Fluorescence spectra of DOX@NM in H_2O with increasing DMSO amount, under (A) 330 nm excitation, and (B) 480 nm excitation. (C) The release of DOX from DOX@NM in H_2O with pure H_2O, 20%,40%, 60% and 80% DMSO and pure DMSO. (D) DOX@NM status coordinate pure H_2O, 20%,40%, 60% and 80% DMSO and pure DMSO. (E) TEM and enlarged view of DOX@NM obtained in pure H_2O, EtOH:H_2O = 1:1, pure EtOH.

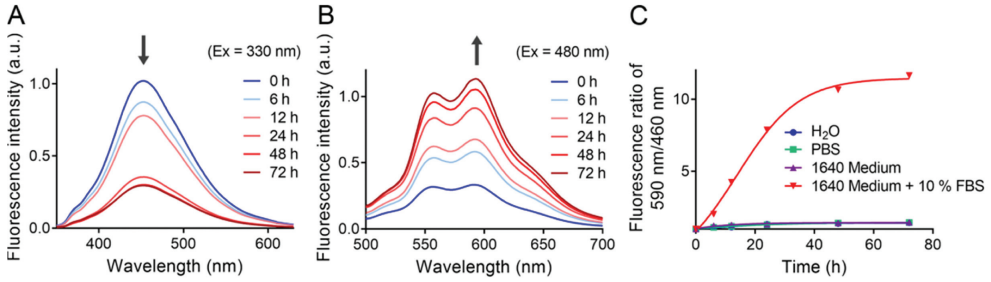

Fig. 3. Fluorescence spectra of DOX@NM in 1640 medium with 10% FBS under (A) 330 nm excitation, and (B) 480 nm excitation. (C) The ratio of 590 nm/460 nm of DOX@NM in different media in 0, 6, 12, 24, 48 and 72 h.

sembled. At the assembled stage (blue color in Fig. 2D), the drug molecule was encapsulated in the hydrophobic core. In this stage, the fluorescent intensity ratio of DOX/TPE is less than 4; While at the disassembling stage, NM are disassembled and DOX is released, the fluorescent intensity ratio of DOX/TPE (590 nm/460 nm) is increased to 4∼40; When the DOX@NM completely disassembled, DOX was released completely (red color in Fig. 2D), the ratio is greater than 40. In TEM, the shapes of DOX@NM are following the three stages analyzed (Fig. 2E). We use different ratios of DOX/TPE (590 nm/460 nm), <4, 4–40, or >40 as references to reveal the DOX@NM stability.

Media effects on DOX@NM were studied. One standard for choosing a medium is that the medium should have neglectable fluorescence background. Based on this, four media were selected: (i) H_2O, (ii) PBS, (iii) 1640 medium, and (iv) 1640 medium with 10% FBS (Fig. S16 in Supporting information). In H_2O, PBS and 1640 medium, DOX@NM was stable. The TPE and DOX fluorescence of DOX@NM did not show obvious changes in 72 h (Fig. S17 in Supporting information). While in (iv) medium, the fluorescence of TPE decreased (Figs. 3A and B). DOX fluorescence intensity recovered. According to the established DOX@NM status coordinate (Fig. 2D), the ratio of 590 nm/460 nm in (iv) medium was greater than 4, indicating DOX@NM was disassembled (Fig. 3C). The FBS could reduce the stability of the DOX@NM and lead to their scatter.

FBS contains most proteins in the blood and small molecules that regulate life activities [39]. It would be of great help for the design and preparation of DOX@NM to clarify which substance in serum contributes most to micellar disassemble. We experimented to find out effects of proteins on the stability of DOX@NM. Albumin and globulin are selected for they are the most important protein components, accounting for 60% and 30% of total blood proteins, respectively [40,41]. Due to the technical limitations of separation and purification, it is nearly impossible to obtain a single α- or β-pure product. So, α-/β-mixed globulin and γ-globulin were used in this experiment. First, albumin and DOX@NM were co-cultured for 24 h, respectively. The fluorescence intensity increased by 3% at 590 nm (Ex under 480 nm) and decreased by 7% at 460 nm (Ex under 330 nm). For α-/β-globulin and DOX@NM system, the fluorescence intensity was enhanced by 15% at 590 nm, and decreased by 18% at 460 nm. The fluorescence of DOX@NM of both systems at 590 nm/460 nm is around 0.3 and 0.8. Both are much less than 4 (Fig. S18 in Supporting information). According to the DOX@NM status coordinate (Fig. 2D), albumin and α-/β-globulin might not be able to make DOX@NM disassemble obviously. Interestingly, for γ-globulin and DOX@NM system, the fluorescence intensities increased by 400% at 590 nm and decreased by 50% at 460 nm, which is much different from the albumin or α-/β-globulin, indicating γ-globulin interacts with DOX@NM much more actively. The fluorescence of DOX@NM at 590 nm/460 nm changes in a 'seesaw-like' behavior when DOX@NM interacts with γ-globulin (Figs. 4A and B). In about 5 h, the ratio of 590 nm/460 nm was increased to 10, as shown in Fig. 4C. From the DOX@NM status coordinate (Fig. 2D), γ-globulin made DOX@NM disassembled. Then, the interaction of DOX@NM with proteins were studied by gel electrophoresis, and Coomassie dye was used for color development (Fig. 4D). Reference bands were measured as: a, pro-

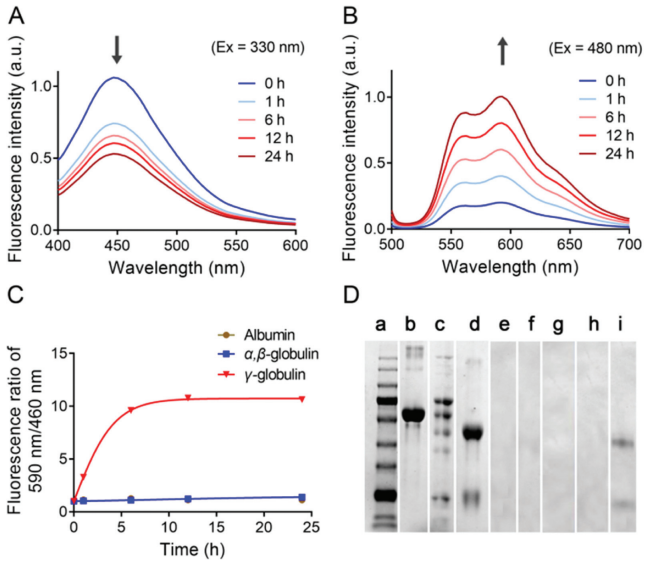

Fig. 4. Fluorescence spectra of DOX@NM with γ-globulin under (A) 330 nm excitation, and (B) 480 nm excitation. (C) The ratio of 590 nm/460 nm of DOX@NM with albumin, α-/β-globulin and γ-globulin in 0, 1, 6, 12 and 24 h. (D) Electrophoretic image of different proteins interacting with DOX@NM (a, protein marker; b, albumin; c, α-/β-globulin; d, γ-globulin; e, NM; f, DOX@NM; g, incubation of DOX@NM with albumin; h, incubation of DOX@NM with α-/β-globulin; i, incubation of DOX@NM with γ-globulin).

tein marker; b, albumin; c, α-/β-globulin; d, γ-globulin; e, NM; f, DOX@NM. We incubated the DOX@NM with albumin, α-/β-globulin and γ-globulin. After separation from free proteins by ultra-high-speed centrifugation, samples were obtained in the upper solution phase. After gel electrophoresis, bands could be observed in (i) DOX@NM + γ-globulin, but not in (h) DOX@NM + α-/β-globulin or (g) DOX@NM + albumin. While in the group (i), the bands were dyed, consistent with those of pure γ-globulin (d). This indicates that DOX@NM could interact with γ-globulin. It is known that α- and β- globulins mostly play act as enzymes, while γ globulins act as immunoglobulins. γ-Globulins' immune-related properties were believed to lead to a strong interaction with DOX@NM. The assumptions were supported by circular dichroism results (Fig. S19 in Supporting information).

We explored the stability properties of DOX@NM *in vivo*. *In vivo*, DOX@NM might encounter complex environment, such as inorganic/organic small molecules, bioactive proteins, high-speed blood flow and various physiological obstacles [42,43]. The UV absorption of whole blood of ICR mice was performed (Fig. 5A). The absorption spectrum of whole blood was relatively complex, with maximum absorption at 414 nm and several minor absorptions. The absorption intensities around the two excitation wavelengths (330 nm and 480 nm) were small and showed no obvious overlap with DOX@NM. Then, the stability of DOX@NM *in vitro* (Figs. 5B and C) and *in vivo* (Figs. 5D and E) blood of mice was studied. As shown in Fig. 5F, the emission wavelength of DOX and TPE molecules are slightly red-shifted, DOX changes from 590 nm to 601 nm, and TPE changes from 460 nm to 487 nm. *In vivo*, it takes about 60 min for the ratio of 601 nm/487 nm to increase greater than 4; *in vitro*, it takes much longer, around 600 min. We take the DOX@NM status coordinate chart as a reference (Fig. 2D). It indicates that both *in vitro* and *in vivo*, blood can gradually disassemble DOX@NM. But, *in vivo*, the blood had a stronger ability to disassemble the DOX@NM. It is believed that the following factors contribute to the effect: shear force generated by high-speed blood flow in blood vessels and the clearance of immune barriers, *e.g.*, macrophages or the reticuloendothelial system in the body. All of these factors make DOX@NM unstable in the body. The study of more details of DOX@NM *in vivo* is still ongoing in our lab.

In summary, AIEgen TPE functionalized polymer TPGS-TPE was synthesized as the building block to assemble nanomicelles NM. Doxorubicin-loaded nanomicelles DOX@NM were prepared. The stability of DOX@NM was studied by 'seesaw-like' fluorescence changes. Based on the changes, we plot a DOX@NM status coordinate. When the DOX@NM were in the assembled form, the fluorescence of DOX was quenched for ACQ effects, and the fluorescence of TPE was observed for its AIE effect; *Vice versa,* when the DOX@NM were in disassembled form, the fluorescence of DOX restored, and AIE fluorescence of TPE molecules disappeared. This fluorescence relationship between AIE polymer and DOX can be used to dynamically study the actual micellar states, which pro-

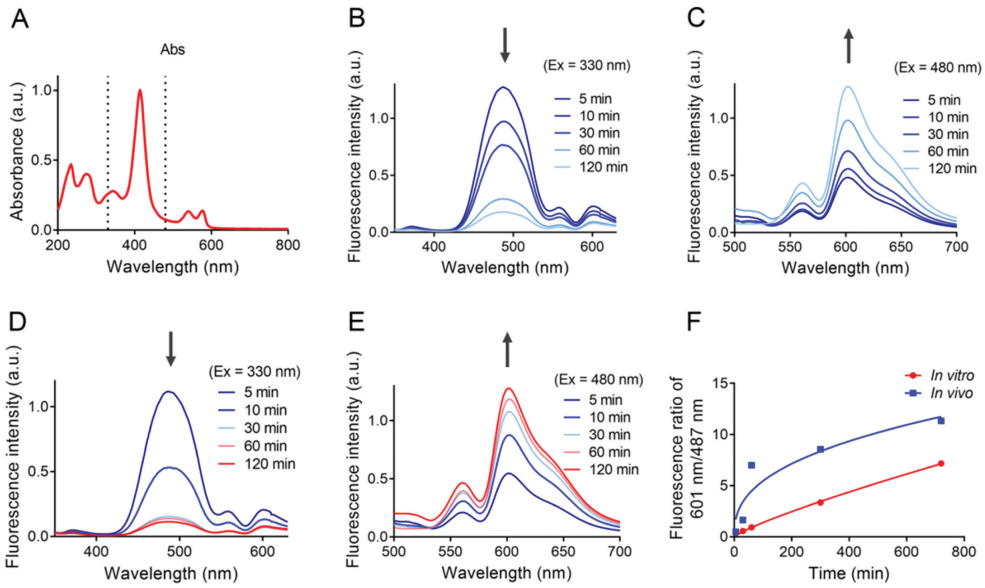

Fig. 5. (A) UV absorption spectrum of the whole blood of mice. Fluorescence spectra of DOX@NM under (B) 330 nm excitation, and (C) 480 nm excitation after *in vitro* blood treatment. Fluorescence spectra of DOX@NM excited at (D) 330 nm and (E) 480 nm after *in vivo* blood treatment. (F) The ratio of Em 601 nm/Em 487 nm in different time *in vitro* and *in vivo*.

vides an approach for exploring the stability of micellar drugs and hopefully accelerate the progress for micellar medicines into clinical uses.

Declaration of competing interest

The authors declare that they have no known competing financial interests or personal relationships that could have appeared to influence the work reported in this paper.

Acknowledgments

This work was supported by the National Natural Science Foundation of China (Nos. 31971304, 22007027), Science Fund for Creative Research Groups of Nature Science Foundation of Hebei Province (No. B2021201038), One Hundred Talent Project of Hebei Province (No. E2020050010), Post-graduate's Innovation Fund Project of Hebei University (No. HBU2022bs011). We are grateful to Medical Comprehensive Experimental Center of Hebei University for the animal experiment. All animal experiments were conducted according to the requirements of the Experimental Animal Ethics Committee of Hebei University.

Supplementary materials

Supplementary material associated with this article can be found, in the online version, at doi:10.1016/j.cclet.2022.107866.

References

[1] V.P. Torchilin, Pharm. Res. 24 (2007) 1–16.
[2] Q. Zhou, T. Zhao, M. Liu, et al., Nano Res. 15 (2022) 4582–4589.
[3] Y. Malam, M. Loizidou, A.M. Seifalian, Trends Pharmacol. Sci. 30 (2009) 592–599.
[4] N. Filipczak, J. Pan, S.S.K. Yalamarty, et al., Adv. Drug Deli. Rev. 156 (2020) 4–22.
[5] J. Cheng, B.A. Teply, I. Sherifi, et al., Biomaterials 28 (2007) 869–876.
[6] J.M. Chan, L. Zhang, K.P. Yuet, et al., Biomaterials 30 (2009) 1627–1634.
[7] A.S. Chauhan, Molecules 23 (2018) 938.
[8] P. Kesharwani, S. Banerjee, U. Gupta, et al., Mater. Today 18 (2015) 565–572.
[9] Q. Liu, B. Wu, M. Li, et al., Adv. Sci. 9 (2022) 2103911.
[10] Z. Deng, C. Jiang, M.R. Younis, et al., Chin. Chem. Lett. 32 (2021) 2411–2414.
[11] M.H. Matsumura Y, Cancer Res. 46 (1986) 6387–6392.
[12] H. Maeda, J. Wu, T. Sawa, et al., J. Control. Release 65 (2000) 271–284.
[13] Y. Zhang, K. Olofsson, Y. Fan, et al., Small 17 (2021) e2007305.
[14] Y. Du, W. Chen, M. Zheng, et al., Biomaterials 33 (2012) 7291–7299.
[15] A. Roloff, A.S. Carlini, C.E. Callmann, et al., J. Am. Chem. Soc. 139 (2017) 16442–16445.
[16] D. Hwang, J.D. Ramsey, A.V. Kabanov, Adv. Drug Deliv. Rev. 156 (2020) 80–118.
[17] A. Mandal, V. Gote, D. Pal, et al., Pharm. Res. 36 (2019) 36.
[18] K.P.W. Shi J, R. Wooster, et al., Nat. Rev. Cancer 17 (2017) 20–37.
[19] P. Zhong, H. Meng, J. Qiu, et al., J. Control. Release 259 (2017) 176–186.
[20] S.C. Owen, D.P.Y. Chan, M.S. Shoichet, Nano Today 7 (2012) 53–65.
[21] S. Kim, Y. Shi, J.Y. Kim, et al., Expert Opin. Drug Deliv. 7 (2010) 49–62.
[22] R. Savić, T. Azzam, A. Eisenberg, et al., Langmuir 22 (2006) 3570–3578.
[23] A. Reisch, A.S. Klymchenko, Small 12 (2016) 1968–1992.
[24] S.W. Morton, X. Zhao, M.A. Quadir, et al., Biomaterials 35 (2014) 3489–3496.
[25] E. Lerner, A. Barth, J. Hendrix, et al., eLife Sciences 10 (2021) e60416.
[26] J. Guo, H. Hong, G. Chen, et al., Biomaterials 34 (2013) 8323–8332.
[27] Y. Hong, J.W.Y. Lam, B.Z. Tang, Chem. Soc. Rev. 40 (2011) 5361–5388.
[28] Y. Zhang, J. Wang, H. Chen, et al., Chin. Chem. Lett. 33 (2022) 2473–2476.
[29] D. Mao, B. Liu, Matter 4 (2021) 350–376.
[30] B. Wu, J. Wang, X. Liu, et al., Nat. Commun. 12 (2021) 3680.
[31] D. Guo, Z. Xu, D. Yang, et al., Nanoscale 12 (2020) 2648–2656.
[32] T. Han, X. Wang, D. Wang, et al., Top. Curr. Chem. 379 (2021) 7.
[33] Y.F. He X, D. Wang, et al., Nano Lett. 19 (2019) 2272–2279.
[34] Z.J. Wang Y, Z. Dong, et al., Mater. Today Chem. 21 (2021) 100537.
[35] W.R. Blomberg, J. Machhi, J. Herskovitz, et al., Biomaterials 231 (2020) 119669.
[36] C. Yang, T. Wu, Y. Qi, et al., Theranostics 8 (2018) 464.
[37] J. Mei, Y. Hong, J.W. Lam, et al., Adv. Mater. 26 (2014) 5429–5479.
[38] K.S. Patil, A.A. Hajare, A.S. Manjappa, et al., J. Drug Deliv. Sci. Technol. 65 (2021) 102685.
[39] E.H. Pilkington, O.J.R. Gustafsson, Y. Xing, et al., ACS Nano 12 (2018) 6066–6078.
[40] A. Aguilera-Garrido, T. del Castillo-Santaella, Y. Yang, et al., Adv. Colloid Interface Sci. 290 (2021) 102365.
[41] R.K. Jagdish, J.S. Maras, S.K. Sarin, Hepatology 74 (2021) 2848–2862.
[42] N. Feiner-Gracia, M. Buzhor, E. Fuentes, et al., J. Am. Chem. Soc. 139 (2017) 16677–16687.
[43] D.W. Malcolm, J.J. Varghese, J.E. Sorrells, et al., ACS Nano 12 (2018) 187–197.